Trapping and Chaining Self-Assembly of Colloidal Polystyrene Particles over Floating Electrode by Using Combined Induced-Charge Electroosmosis and Attractive Dipole-Dipole Interaction – supplementary information

Weiyu Liu,[a] Jinyou Shao,[a,*] Yankai Jia,[b] Ye Tao,[b] Yucheng Ding,[a] Hongyuan Jiang,[b] and Yukun Ren[b,*]

[a]Micro and Nano-technology Research Center, State Key Laboratory for Manufacturing Systems Engineering, Xi'an Jiaotong University, Xi'an, Shaanxi, China 710049
[b]School of Mechatronics Engineering, Harbin Institute of Technology, West Da-zhi Street 92, Harbin, Heilongjiang, P. R. China 150001

Theory

Quasi-electrostatics

Considering electro-neutrality for the bulk solution in the absence of magnetic effects, the set of Maxwell equations is reduced to

$$\begin{cases} \rho_V = \nabla\cdot(\varepsilon \boldsymbol{E}) \\ \dfrac{\partial \rho_V}{\partial t} + \nabla\cdot(\sigma \boldsymbol{E}) = 0 \\ \boldsymbol{E} = -\nabla\phi \end{cases} \tag{S1}$$

Here $\boldsymbol{E}$ is an applied electric field, ϕ the bulk potential, ρ_V a distribution of volumetric free charge density existing only in the presence of any dielectric gradient across the bulk.[1-5] ε and σ are dielectric permittivity and electrical conductivity, respectively. Assuming a harmonic actuation $\phi(t) = A\cos(\omega t + \theta)$ and hence seeking solution for sinusoidal steady state, we introduce phasor amplitude of each electric field variable denoted by a tilde for analytical convenience

$$\begin{aligned} \phi(t) &= A\cos(\omega t + \theta) \\ &= \mathrm{Re}\left(Ae^{j\theta}e^{j\omega t}\right) = \mathrm{Re}\left(\tilde{\phi}e^{j\omega t}\right) \end{aligned} \tag{S2a}$$

$$\boldsymbol{E}(t) = \mathrm{Re}\left(\tilde{\boldsymbol{E}}e^{j\omega t}\right) \tag{S2b}$$

$$\rho(t) = \mathrm{Re}\left(\tilde{\rho}e^{j\omega t}\right) \tag{S2c}$$

Here $\omega = 2\pi f$ and f are the angular frequency and linear frequency of the harmonic field, respectively.

From Eq.(S1) and Eq.(S2), charge conservation for sinusoidal steady state is obtained

$$\nabla\cdot\left((\sigma + j\omega\varepsilon)\tilde{\boldsymbol{E}}\right) = 0 \tag{S3}$$

For homogeneous bulk salt concentration, Eq.(S3) is further reduced to the Laplace equation[6, 7]

$$\nabla^2\tilde{\phi} = 0 \tag{S4}$$

AC Dielectrophoresis (DEP)

At frequency below tens of megahertz, Maxwell-Wagner interfacial polarization is the dominating polarization mechanism at the interface between two dielectrics.[8] When a dielectric particle suspended in liquid medium of different polarizabilities is subjected to a background non-uniform electric field $\boldsymbol{E}$, DEP force acting on the induced dipole moment of the particle will attract it to (positive DEP or pDEP, $\mathrm{Re}\left(f_{CM}(\omega)\right) > 0$) or repel it away from (negative DEP or nDEP, $\mathrm{Re}\left(f_{CM}(\omega)\right) < 0$) a high field intensity region.

Point dipole approximation

For spherical particles of radius R, the net time-averaged DEP force in an AC field can be given by the point dipole (PD) approximation which ignores any near-field effect[9-12]

$$\langle \boldsymbol{F}_{DEP} \rangle = \pi \varepsilon_f R^3 \,\mathrm{Re}\left(f_{CM}(\omega)\right) \nabla \left(\overset{\circ}{\boldsymbol{E}} \cdot \overset{\circ}{\boldsymbol{E}}^{*} \right) \qquad \text{(S5)}$$

With $f_{CM}(\omega)$ being the frequency-dependent Clausius-Mossotti (C-M) factor[13-15]

$$f_{CM}(\omega) = \frac{\overset{\pm}{\varepsilon}_p - \overset{\pm}{\varepsilon}_f}{\overset{\pm}{\varepsilon}_p + 2\overset{\pm}{\varepsilon}_f} \qquad \text{(S6)}$$

Here Re(…) denotes the real part of (…), and * is the complex conjugate operator. The subscripts p and f represent particle and fluid, respectively. $\overset{\pm}{\varepsilon}_{p,f} = \varepsilon_{p,f} - j\dfrac{\sigma_{p,f}}{\omega}$ is the complex permittivity of an indexed lossy dielectric.

Since they possess a net surface charge density, PS particles at nano- and micro-meter dimension do not behave as ideal insulators. An equivalent bulk conductivity of the PS colloids is related to the surface conductance Ks through

$$\sigma_p = \frac{2Ks}{R} = \frac{2\times10^{-9}\,S}{5\times10^{-6}\,\mathrm{m}} = 0.0004\,S/m \qquad \text{(S7)}$$

Here $Ks = 1nS$ is appropriate for particle diameter more than 2μm.[9] $0.0004\,S/m$ PS particle of 5μm radius suspended in $0.002\,S/m$ electrolyte gives rise to an in-phase polarization shown in Figure S1(A), which has a constant low-frequency conductivity plateau around -0.363 from 1Hz to 10kHz. As a result, any frequency-dependent particle behaviours observed in this frequency range cannot be solely caused by Maxwell-Wagner interfacial charge relaxation.

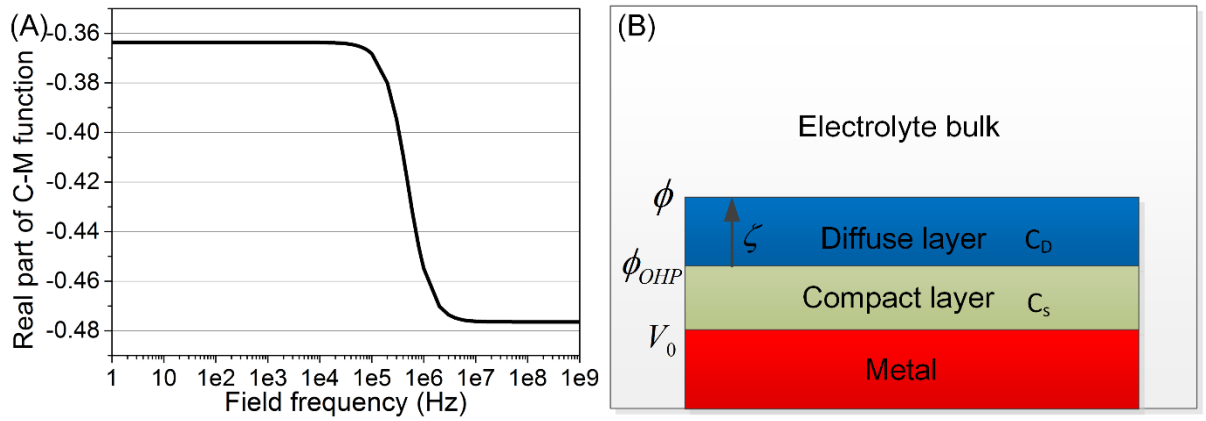

Figure S1. (A) Real part of the C-M factor for 10μm PS microbeads suspended in 0.002S/m electrolyte solution; (B) Double-layer model: a stern-layer capacitance C_s is in series with the diffuse-layer capacitance C_D with a surface capacitance ratio $\delta = C_D/C_S$.

Maxwell stress tensor approach

If any near-field influence becomes important, such as particles come close to one another or any other solid surface, the above approximation can no longer work accurately. Under such circumstances, the DEP force can be accurately obtained by integrating the time-averaged Maxwell stress tensor (MST) over the control surface of a closed volume[16, 17]

$$\langle \boldsymbol{F}_{DEP} \rangle = \oint_{\partial P} \left\langle \overset{\$}{T} \right\rangle \cdot \boldsymbol{n} dS \qquad \text{(S8)}$$

Here $\boldsymbol{n}$ is the unit vector normal to the particle surface ∂P .

The expression of MST is given by

$$\left\langle \overset{\$}{T} \right\rangle = \frac{\varepsilon_f}{2} \mathrm{Re}\left(\overset{\pm}{\boldsymbol{E}}_f \overset{\pm}{\boldsymbol{E}}_f^{\,*} - \frac{1}{2}\left(\overset{\pm}{\boldsymbol{E}}_f \cdot \overset{\pm}{\boldsymbol{E}}_f^{\,*} \right) \mathbf{I} \right) \qquad \text{(S9)}$$

Here the subscript f means the complex electric field $\overset{\pm}{\boldsymbol{E}}_f$ is obtained in the fluid domain along the control surface ∂P , and $\mathbf{I}$ is a unit tensor.

Continuity of normal component of the complex electric displacement vector is satisfied across the particle/electrolyte interface ∂P

$$\begin{cases} \left(\sigma_p + j\omega\varepsilon_p\right)\left.\dfrac{\partial \phi}{\partial n}\right|_p = \left(\sigma_f + j\omega\varepsilon_f\right)\left.\dfrac{\partial \phi}{\partial n}\right|_f \\ \left.\phi\right|_p = \left.\phi\right|_f \end{cases} \qquad \text{(S10)}$$

Field-induced double-layer polarization

An initial normal field component on the surface of the floating electrode brings mobile counter-ions to this interface (Figure 1(C)), where they accumulate and form a diffuse screening cloud of dipolar nature after a characteristic RC charging time $\tau_{RC} = aC_d/\sigma_f\left(1+\delta\right) = \varepsilon a/\sigma_f\lambda_D\left(1+\delta\right)$($a = 0.195L = 39\mu\text{m}$ is the characteristic macroscopic length scale).[18] This IDL has a Debye length $\lambda_D = \sqrt{D\varepsilon_f/\sigma_f} \approx 26.6nm$.[8, 19, 20] Here $D = 2\times10^{-9}m^2/\text{s}$ is the ionic diffusivity.

As for mathematical description of field-induced double-layer polarization around the floating electrode, the diffuse screening cloud can be regarded as a capacitor skin charged by Ohmic current from the bulk resistance in the asymptotic limit of thin IDL[21]

$$\sigma_f\left(\boldsymbol{n}\cdot\nabla\phi\right) = j\omega\frac{C_D}{1+\delta}\left(\phi - \mathring{V}_0\right) \qquad \text{(S11)}$$

Here $\delta = \dfrac{C_D}{C_S}$ is the surface capacitance ratio of the diffuse layer $C_D = \dfrac{\varepsilon_f}{\lambda_D}$ to the compact layer $C_S = 0.2F/m^2$, $\mathring{V}_0 = A/2$ the floating potential of the middle electrode, ϕ the potential in the bulk just outside the double-layer, $C_0 = \dfrac{C_D}{1+\delta}$ the interfacial total capacitance (Figure S1(B)), and $\boldsymbol{n}$ the unit normal vector on the surface of the floating electrode.

At steady state, the uneven distribution of an induced surface charge density $-q = -C_0\left(\mathring{V}_0 - \phi\right)$ in the IDL repels the bulk field lines completely, which makes the polarizable surface behave like an insulator (Figure 1(D)).

Induced-charge electroosmotic flow

The action of a tangential field component on the mobile ions in the Debye layer induces ICEO slip velocity $\boldsymbol{u}_{slip}$ on the polarizable electrode surface, the time-averaged expression of which is derivable from the generalization of Helmholtz-Smoluchowski formula[21, 22]

$$\left\langle \boldsymbol{u}_{slip} \right\rangle = \frac{1}{2}\frac{\varepsilon_f}{\eta}\frac{1}{1+\delta}\text{Re}\left(\left(\phi - \mathring{V}_0\right)\left(\mathring{\boldsymbol{E}} - \mathring{\boldsymbol{E}}\cdot\boldsymbol{n}\cdot\boldsymbol{n}\right)^*\right) \qquad \text{(S12)}$$

Here $\eta = 0.001Pa\cdot s$ is the dynamic viscosity of liquid suspension, and $\mathring{\boldsymbol{E}}_t = \mathring{\boldsymbol{E}} - \mathring{\boldsymbol{E}}\cdot\boldsymbol{n}\cdot\boldsymbol{n}$ the tangential component of electric field vector on the electrode surface.

Eq.(S12) is then inserted into the following Stokes equation as the boundary condition on the surface of the bipolar electrode, with all other surfaces being treated as no-slip walls to obtain the steady state ICEO convective flow

$$\begin{cases} -\nabla p + \nabla\cdot\left(\eta\left(\nabla\boldsymbol{u} + \left(\nabla\boldsymbol{u}\right)^T\right)\right) = 0 \\ \nabla\cdot\boldsymbol{u} = 0 \end{cases} \qquad \text{(S13)}$$

Here p is the hydraulic pressure, and $\boldsymbol{u}$ the flow velocity vector.

As shown in Figure 1(D), the ICEO flow has two opposite eddies around the oppositely charged metal strip, and affects the particle electrokinetic motion at low frequencies through the interaction between the hydrodynamics and electrostatics. However, when the field frequency is far beyond the reciprocal RC charging time $f_{RC-average} = \sigma_f\left(1+\delta\right)/2\pi C_d\left(0.195L\right) = 347Hz$ for the equivalent circuit of the bulk ohmic resistance coupled to the interfacial *total* capacitance, there is not enough time for the IDL to form due to a relaxation process. As a consequence, the polarizable metal surface recovers to an ideal conductor above $f_{RC-average}$ (Figure 1(C)), and ICEO flow velocity declines by 50% at $f_{RC-average} = 347\text{Hz}$ (Figure 5(C)).

Numerical simulation

A commercial FEM software package COMSOL 4.4 is used in this study to numerically calculate the particle DEP force and ICEO flow. The electrostatics and hydrodynamics are governed by Eq.(S3) and Eq.(S13), respectively, and boundary conditions for their simulations are shown in Table S1 and Figure S2.

When DEP force is approximated by PD method Eq.(S5), the influence of particle on the its surrounding electric field must be neglected, i.e. Eq.(S10) is not considered and hence Eq.(S3) is solved in the absence of particles. In contrast, when MST approach Eq.(S8) is applied to quantify the accurate DEP force acting any solid body, the impact of the colloid volume on the near-field of the colloid must be directly taken into account in the calculation of the complex electric field.

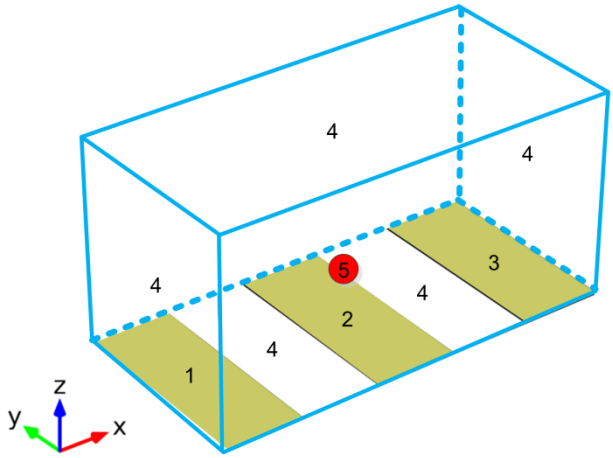

Figure S2. 3-D geometrical model for numerical simulation

Table S1. Boundary conditions for electrostatics and hydrodynamics in numerical simulation

Index number	Name	Electric boundary condition for Eq.(S3)	Flow boundary condition for Eq.(S13)
1	Left electrode	Φ=A	u=0
2	Floating electrode	Eq.(S11)	Eq.(S12)
3	Right electrode	Φ=0	u=0
4	Channel walls	$n\cdot\nabla\Phi$=0	u=0
5	Particle surface	Eq.(S10)	u=0

Particle-electrode electrokinetic interaction

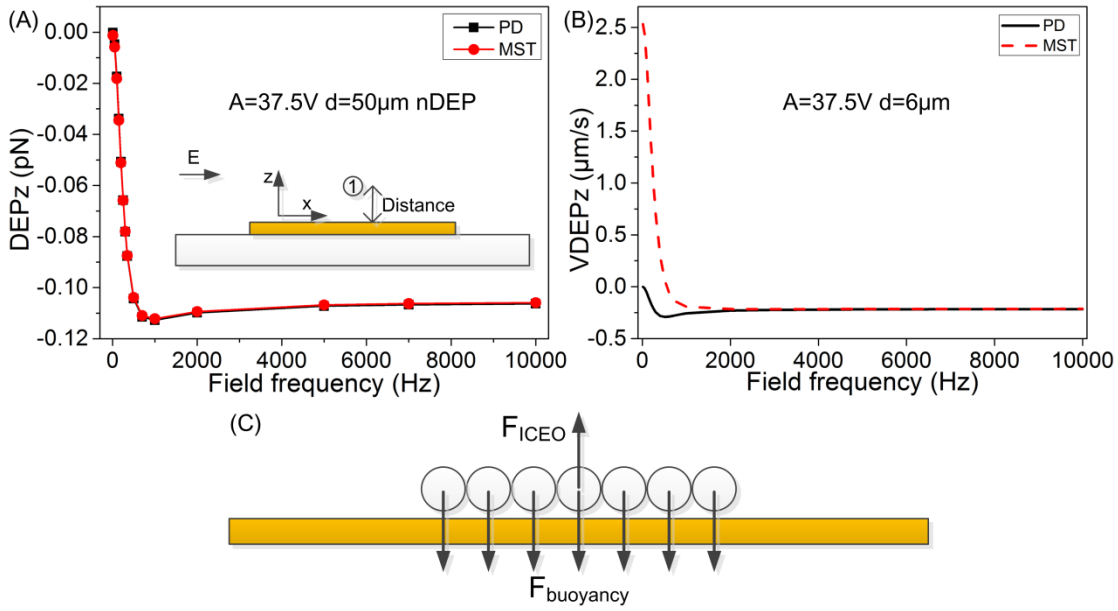

Figure S3. (A) z- component of DEP force (DEPz) acting on particle 1 at a distance of d=50μm from the electrode surface as a function of frequency; (B) z- component of DEP velocity of particle 1 (VDEPz) for d=6μm; (C) Illustration of vertical force components acting on the ensemble of the horizontal particle chain assembled on the electrode surface at 5~50Hz.

As shown in Figure S3(A), the location of particle 1 is chosen in a way that the center of particle 1 has a distance d from the surface of the floating electrode. We need validate the correctness of current MST calculation algorithm in the absence of any near-field effect, so d=50μm much larger than particle radius is preferred. The results from PD approximation and MST method show a good agreement in Figure S3(A). The frequency-dependence of DEP force is due to field-induced double-layer polarization rather than Maxwell-Wagner interfacial relaxation, since the real part of C-M function has a constant low-frequency plateau below 10kHz (Figure S1(A)). Specifically, z- component of DEP force (DEPz) reaches zero in a uniform field around a flat insulator at low frequencies (Figure 1(D)). With increasing field frequency, the floating electrode gradually recovers from an 'insulator' (Figure S4(A)) to a conductor (Figure S4(B)) from the perspective of an observer, resulting in an increase in DEP force. The minus sign in Figure S3(A) indicates DEPz is directed along the negative z axis, i.e. nDEP force attracts the particle to the electrode surface, which is in good agreement with Figure 5(B).

We then investigate particle-electrode electrokinetic interaction by placing particle 1 in close proximity to the electrode surface, e.g. d=6μm. MST method and PD approximation coincide well with each other above 2000Hz, and both of them indicate nDEP velocity on the order of -0.2μm/s toward the electrode center above 500Hz (Figure S3(B)).

However, there is large disparity between the two approaches at low frequencies. Though VDEPz predicted by PD approximation vanishes in DC limit in Figure S3(B) as DEPz does in Figure S3(A), VDEPz predicted by MST method clearly indicates an electrostatic repulsion force (ERF) at low frequencies that repels the colloid away from the electrode surface. In this case, the electrode behaves as insulating channel wall at low frequencies since the electric current passes around it (Figure 1(D)), and the background field is rather uniform. As a result, this ERF has its origin in the near-field non-uniformity caused by the close proximity of the insulating colloidal particle to the 'insulating' electrode (Figure S4(A)). Moreover, we even alter the bulk conductivity of the particle to see if the sign of DEP force can make a change (results no shown here). Even for a conductive particle of $\mathrm{Re}\left(f_{CM}\left(\omega\right)\right)=1$, this DEP force at low frequencies is still repulsive, and there is a special case that ERF is zero when the conductivity of particle equals that of liquid suspension, so ERF acting on colloidal particles which repels them away from insulating walls in a uniform background field is common and independent of particle polarizability.

Analysis of the 2D assembly state

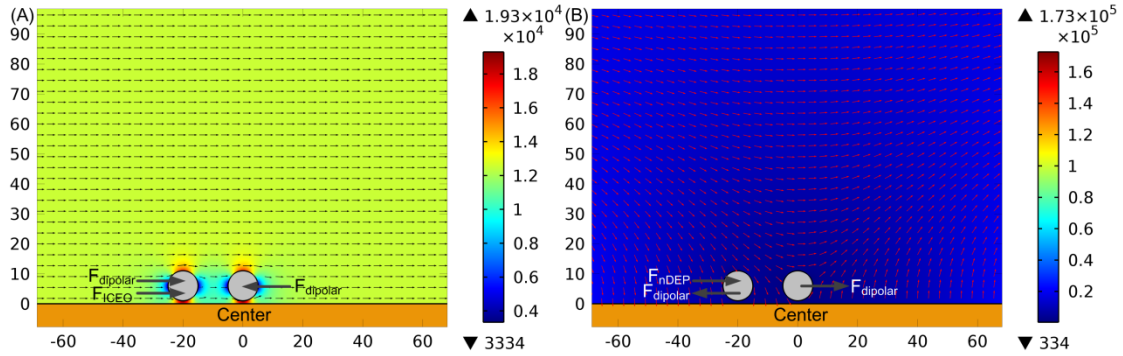

Figure S4. A surface and arrow plot of the electric field in the x-z plane (unit: V/m), influence of dipole-dipole interaction on the near-field of particles, and an illustration of various forces acting on neighbouring colloids under different conditions: (A) at 10Hz and 37.5V; (B) at 10kHz and 62.5V. F_{ICEO}, $F_{dipolar}$ and F_{nDEP} denote ICEO fluidic drag, dipolar interaction and nDEP force, respectively.

Table S2. DEP particle-particle interaction characteristics at different assembly frequencies

Field frequency	x-component (horizontal) DEP interaction F_{DEPx}	y-component DEP interaction F_{DEPy}	The resulting assembly state on the electrode surface
5~50Hz (Figure 2)	Strong attraction	Strong repulsion	*Dipole-dipole chaining* configuration with obvious inter-chain separation
3kHz (Figure 4(B))	Weak attraction	Weak repulsion	*Compact* assembly
10kHz (Figure 4(D))	Weak repulsion	Weak repulsion	*Disordered 2D packing*

Description of video clip

We also include herein a series of video clips of frequency-dependent particle electrokinetic behaviors near the floating electrode to help present our work vividly.

The following is the description of video clip, which are presented in the order of increasing field frequency.

1) At the field frequency 5Hz much lower than the reciprocal RC charging time, ICEO micro-vortices result in a rapid transport of colloidal particles toward the electrode center, where they form arrays of horizontal particle chains that are almost parallel with the applied field direction, and there is large inter-chain separation along the y-direction.
2) At the frequency 10Hz or 50Hz, the particle trapping and *dipolar chaining* self-assembly phenomena keep identical with 5Hz, but the inter-chain distance overall decreases.
3) At 200Hz around the inverse RC time scale, particles or short particle chains formed during rotation rotate synchronously with ICEO vortices in the x-z plane and no particles can be trapped on the electrode surface.
4) At 600Hz, the particle/chain rotation phenomenon keeps similar with 200Hz, but 1~2 columns of particles are trapped on the electrode surface.
5) At 2kHz, some local circulating motion of particles in the vicinity of electrode edge still occurs, and 2~3 columns of particles are trapped on the electrode surface.
6) At 3kHz, particles can be once again effectively trapped at the electrode center under the combined action of ICEO flow and nDEP force, and a *compact* 2D assembly state occurs on the electrode surface.
7) At 10kHz much higher than the characteristic RC charging frequency, nDEP induced particle trapping also takes place at the center of the electrode surface, while *disordered* 2D packing is formed this time.

References for supporting information

S1. W. Liu, Y. Ren, J. Shao, H. Jiang and Y. Ding, *Journal of Physics D: Applied Physics*, 2014, **47**, 075501.
S2. A. Ramos, H. Morgan, N. G. Green and A. Castellanos, *Journal of Physics D: Applied Physics*, 1998, **31**, 2338.
S3. A. Kumar, J.-S. Kwon, S. J. Williams, N. G. Green, N. K. Yip and S. T. Wereley, *Langmuir*, 2010, **26**, 5262-5272.
S4. S. J. Williams, A. Kumar and S. T. Wereley, *Lab Chip*, 2008, **8**, 1879-1882.
S5. M. Stubbe, A. Gyurova and J. Gimsa, *Electrophoresis*, 2013, **34**, 562-574.
S6. K. Yang and J. Wu, *Biomicrofluidics*, 2010, **4**, 034106.
S7. N. G. Green, A. Ramos, A. Gonzalez, H. Morgan and A. Castellanos, *Physical review E*, 2002, **66**, 026305.
S8. A. Ramos, *Electrokinetics and electrohydrodynamics in microsystems*, Springer Science & Business Media, 2011.
S9. H. Morgan and N. G. Green, *AC electrokinetics: colloids and nanoparticles*, Research Studies Press, 2003.
S10. P. K. Wong, C.-Y. Chen, T.-H. Wang and C.-M. Ho, *Analytical chemistry*, 2004, **76**, 6908-6914.
S11. J. Gao, M. L. Sin, T. Liu, V. Gau, J. C. Liao and P. K. Wong, *Lab on a Chip*, 2011, **11**, 1770-1775.
S12. O. D. Velev and K. H. Bhatt, *Soft Matter*, 2006, **2**, 738-750.
S13. J. Gimsa, *Bioelectrochemistry*, 2001, **54**, 23-31.
S14. S. Gupta, R. G. Alargova, P. K. Kilpatrick and O. D. Velev, *Soft Matter*, 2008, **4**, 726-730.
S15. S. Gangwal, A. Pawar, I. Kretzschmar and O. D. Velev, *Soft Matter*, 2010, **6**, 1413-1418.
S16. D. H. Lee, C. Yu, E. Papazoglou, B. Farouk and H. M. Noh, *Electrophoresis*, 2011, **32**, 2298-2306.
S17. B. Bharti and O. D. Velev, *Langmuir*, 2015, DOI: 10.1021/la504793y.
S18. G. Hu and D. Li, *Chemical Engineering Science*, 2007, **62**, 3443-3454.
S19. A. Castellanos, A. Ramos, A. Gonzalez, N. G. Green and H. Morgan, *Journal of Physics D: Applied Physics*, 2003, **36**, 2584.
S20. J. Wu, Y. Ben, D. Battigelli and H.-C. Chang, *Industrial & engineering chemistry research*, 2005, **44**, 2815-2822.

S21. Y. Ren, W. Liu, Y. Jia, Y. Tao, J. Shao, Y. Ding and H. Jiang, *Lab on a Chip*, 2015, **15**, 2181-2191.
S22. P. García-Sánchez, A. Ramos, A. González, N. G. Green and H. Morgan, *Langmuir*, 2009, **25**, 4988-4997.